

# UCLA

## UCLA Previously Published Works

### Title

Mathematical modeling of mutant transferrin-CRM107 molecular conjugates for cancer therapy

### Permalink

<https://escholarship.org/uc/item/9nn892z3>

### Authors

Yoon, Dennis J  
Chen, Kevin Y  
Lopes, André M  
et al.

### Publication Date

2017-03-01

### DOI

10.1016/j.jtbi.2017.01.008

Peer reviewed



# HHS Public Access

Author manuscript

*J Theor Biol.* Author manuscript; available in PMC 2018 March 07.

Published in final edited form as:

*J Theor Biol.* 2017 March 07; 416: 88–98. doi:10.1016/j.jtbi.2017.01.008.

## Mathematical Modeling of Mutant Transferrin-CRM107 Molecular Conjugates for Cancer Therapy

Dennis J. Yoon<sup>a</sup>, Kevin Y. Chen<sup>a</sup>, André M. Lopes<sup>a</sup>, April A. Pan<sup>a</sup>, Joseph Shiloach<sup>b</sup>, Anne B. Mason<sup>c</sup>, and Daniel T. Kamei<sup>a,\*</sup>

<sup>a</sup>Department of Bioengineering, University of California, Los Angeles, 420 Westwood Plaza, 5121 Engineering V, Los Angeles, CA 90095, USA

<sup>b</sup>Biotechnology Core Laboratory, National Institute of Diabetes and Digestive and Kidney Diseases, National Institute of Health, Bethesda, MD 20892, USA

<sup>c</sup>Department of Biochemistry, University of Vermont College of Medicine, Burlington, VT 05405, USA

### Abstract

The transferrin (Tf) trafficking pathway is a promising mechanism for use in targeted cancer therapy due to the overexpression of transferrin receptors (TfRs) on cancerous cells. We have previously developed a mathematical model of the Tf/TfR trafficking pathway to improve the efficiency of Tf as a drug carrier. By using diphtheria toxin (DT) as a model toxin, we found that mutating the Tf protein to change its iron release rate improves cellular association and efficacy of the drug. Though this is an improvement upon using wild-type Tf as the targeting ligand, conjugated toxins like DT are unfortunately still highly cytotoxic at off-target sites. In this work, we address this hurdle in cancer research by developing a mathematical model to predict the efficacy and selectivity of Tf conjugates that use an alternative toxin. For this purpose, we have chosen to study a mutant of DT, cross-reacting material 107 (CRM107). First, we developed a mathematical model of the Tf-DT trafficking pathway by extending our Tf/TfR model to include intracellular trafficking via DT and DT receptors. Using this mathematical model, we subsequently investigated the efficacy of several conjugates in cancer cells: DT and CRM107 conjugated to wild-type Tf, as well as to our engineered mutant Tf proteins (K206E/R632A Tf and K206E/R534A Tf). We also investigated the selectivity of mutant Tf-CRM107 against non-neoplastic cells. Through the use of our mathematical model, we predicted that (i) mutant Tf-CRM107 exhibits a greater cytotoxicity than wild-type Tf-CRM107 against cancerous cells, (ii) this improvement was more drastic with CRM107 conjugates than with DT conjugates, and (iii) mutant Tf-CRM107 conjugates were selective against non-neoplastic cells. These predictions were validated with *in vitro* cytotoxicity experiments, demonstrating that mutant Tf-CRM107

\*Corresponding author: 420 Westwood Plaza, 5121J Engineering V, University of California, Los Angeles, CA 90095-1600, USA. Tel.: +310 206 4826. kamei@seas.ucla.edu.

**Publisher's Disclaimer:** This is a PDF file of an unedited manuscript that has been accepted for publication. As a service to our customers we are providing this early version of the manuscript. The manuscript will undergo copyediting, typesetting, and review of the resulting proof before it is published in its final citable form. Please note that during the production process errors may be discovered which could affect the content, and all legal disclaimers that apply to the journal pertain.

conjugates is indeed a more suitable therapeutic agent. Validation from *in vitro* experiments also confirmed that such whole-cell kinetic models can be useful in cancer therapeutic design.

## Keywords

diphtheria toxin; drug delivery; targeted toxin

## 1 Introduction

Cancer is the second leading cause of death in the United States, with over 1.6 million new cancer cases and 590,000 deaths in the country every year (Siegel et al., 2016). Though traditional treatments such as chemotherapy can be effective, they frequently cause dangerous side effects due to nonspecific off-target toxicity. One method to improve targeted drug delivery is through the use of drugs conjugated to transferrin (Tf). Human serum Tf is a monomeric glycoprotein with a molecular weight of approximately 80 kDa, which is involved in transporting iron to the cells in the body. Because of the overexpression of the transferrin receptor (TfR) on a variety of metastatic cells (Daniels et al., 2006), Tf has been investigated as a potential targeting agent for cancer treatment (Cazzola et al., 1990; Ponka and Lok, 1999). Though Tf has been shown to be effective in targeting cancerous cells, its ability to delivery therapeutics is often limited by its inherent TfR-mediated intracellular trafficking pathway. For example, the entire Tf cycle has been shown to last only ~5 min in a human erythroleukemia-derived cell line (K562 cells), and therefore, 30 successive cycles of Tf-toxin conjugate trafficking would be needed before the cytotoxicity on the cell can be observed (Johnson et al., 1988; Klausner et al., 1983a). Furthermore, after iron-loaded Tf (holo-Tf) delivers its iron payload within the cell, the iron-free Tf (apo-Tf) has significantly reduced binding affinity to TfR outside the cell, and therefore, is unable to re-enter the trafficking pathway until it can bind to free iron, which is not an efficient process (Ciechanover et al., 1983; Qian et al., 2002; Yadi and Murphy, 1994). While the cycle demonstrates evolutionary efficiency for rapidly delivering large quantities of iron to cells, this short duration limits the window of opportunity for Tf to deliver a cytotoxic payload.

To identify a molecular-level design criterion to increase the time Tf spends with the cell (*i.e.*, increase its cellular association) and predict trends, our laboratory previously developed a mathematical model of the Tf/TfR intracellular trafficking pathway based on the principles of mass action kinetics (Lao and Kamei, 2008; Lao et al., 2007). Through analysis of the model, our research group discovered that an increase in cellular association could be accomplished by inhibiting the iron delivery rate of Tf. We subsequently demonstrated that two engineered Tf mutants (K206E/R632A Tf and K206E/R534A Tf) with reduced iron release rates dramatically increased cellular association in HeLa and glioma cells. These Tf mutants were then conjugated to DT, and the mutant Tf-DT conjugates were significantly more cytotoxic than the wild-type Tf-DT conjugate when administered to HeLa and glioma cells (Yoon et al., 2010, 2009). Though these mutant Tf conjugates with DT were effective against cancer cells, they cannot be utilized clinically due to the potential of DT to cause toxicity at off-target sites. It has been suggested that only a few micrograms of DT cause death in an unimmunized human (Collier, 1975). In fact, our previous studies have shown

that a conjugate concentration lower than  $3.16 \times 10^{-11}$  M will cause cell death (Yoon et al., 2010). Thus, an alternative drug to DT must be investigated for clinical treatment.

In this work, we aimed to address this challenge by developing a mathematical model that can predict the behavior of other toxins conjugated to Tf. For this theoretical investigation of a novel conjugate, we chose to study a mutant of DT known as cross-reacting material 107 (CRM107). CRM107 is identical to DT but with two point mutations that decrease its binding affinity to its native receptor, heparin-binding epidermal growth factor precursor (preHB-EGF), by 8,000 fold (Johnson et al., 1989). The reduction in binding affinity to this DT receptor (DTR) can potentially lower nonspecific toxicity. In addition, unlike other toxins with negligible toxic side effects, *e.g.*, saporin and gelonin, CRM107 maintains the inherent membrane translocation activity of DT, providing CRM107 with a means of endosomal escape upon cellular internalization. By facilitating its localization to the cytosol, its site of action, the efficacy of the toxin following receptor-mediated endocytosis is greatly improved. Thus, CRM107 has the potential for reducing nonspecific toxicity at off-target sites while maintaining toxicity in tumor cells. Furthermore, our prior experience with DT allows us to translate our mutant Tf-DT conjugate formulation and characterization methods to CRM107.

We modeled the Tf-toxin conjugates by extending our previous Tf/TfR trafficking model to include the DT/DTR trafficking pathway. Figure 1 shows the transferrin-related trafficking parameters associated with ligand/receptor and ligand/metal interactions that we have previously investigated (Lao et al., 2007). Holo-Tf first binds to its receptor on the cell surface at a rate of  $k_{FeTf, TfR}$ , and is internalized at a rate of  $k_{int, Tf}$ . The iron can then be released from the transferrin ( $k_{Fe, rel}$ ), and apo-Tf is either degraded ( $k_{deg, Tf}$ ) or recycled to the surface ( $k_{rec}$ ). To account for DT and its mutant, CRM107, the DT/DTR trafficking pathway (Figure 2) was investigated. The Tf-DT conjugates can enter via the DT pathway through DT binding to its native receptor ( $k_{DT}$ ) and being internalized ( $k_{int, DT}$ ). The catalytic domain of DT (DTA) is then separated from its receptor-binding and translocation domains (DTB) and translocated into the cytosol ( $k_{trans}$ ), where the toxin kills the cell. The DT receptor is then degraded ( $k_{deg}(1-f_{DT})$ ), where  $f_{DT}$  is the fraction of internalized DT sorted for translocation. Species balances associated with this combined Tf-DT trafficking model can be found in the Supplementary Information.

In this study, we used our mathematical model of the Tf-DT intracellular trafficking pathway to investigate the cytotoxicity of native Tf and our mutant Tf (K206E/R632A Tf and K206E/R534A Tf) conjugated to DT and CRM107. These simulations were performed to theoretically examine the use of mutant Tf as a targeting ligand for CRM107 and investigate the efficacy of those conjugates against cancer cells, as mutant Tf-CRM107 conjugates are assumed to only enter cells through the Tf/TfR trafficking pathway. We also used the mathematical model to investigate whether or not changing the toxin moiety of our Tf-based therapeutic agent to CRM107 actually results in selectivity against normal cells and an improved therapeutic index. These mathematical predictions were then validated using *in vitro* studies in various cancerous and non-cancerous cell lines.

## 2 Materials and Methods

### 2.1 Mathematical model of DT/DTR intracellular trafficking

A DT/DTR intracellular trafficking model was derived using the principles of mass action kinetics and was incorporated into our previous Tf/TfR model. The assumptions for this model are listed below, as are the species balances associated with this extension. Model parameters are discussed in this section as well.

**2.1.1 Model Assumptions**—The behavior of this model was defined through several assumptions as described below.

- i.** The total number of DTR was assumed to be constant, as an equal number of DTR was assumed to be synthesized by the cell as was degraded.
- ii.** The DTR is typically processed by one of two ways. It is either proteolytically processed into its mature soluble form, or it is internalized into the cell for degradation (Goishi et al., 1995). DTR turnover occurs primarily through this latter internalization pathway. The model assumed that the proteolytic processing of DTR is negligible. The model also assumed that the internalization rate was the same for free and DT-bound DTR, since it is believed that DT enters cells by hijacking this inherent internalization pathway of DTR.
- iii.** Internalized DTR was assumed to only follow the lysosomal degradation pathway upon clathrin-dependent internalization. This is supported by studies of the effects of protein biosynthesis inhibitors on the DT/DTR trafficking cycle. These studies demonstrate that inhibition of cellular protein biosynthesis prevents the recovery of steady-state levels of cell-surface DTR following internalization. Cell-surface levels of this protein are re-established to steady-state levels upon removal of the inhibitor, suggesting DTR must be constantly re-synthesized (Ronnberg and Middlebrook, 1989).
- iv.** It was assumed that once the DT/DTR complex is internalized, DT does not dissociate from its receptor
- v.** It was assumed that once the catalytic domain of DT (DTA) is separated from its receptor-binding and translocation domains (DTB) and released into the cytosol, it was not inactivated or degraded within the timeframe of the model simulation. This is supported by experiments demonstrating that more than 80% of DTA directly injected into the cytosol of Ehrlich ascites tumor cells can be recovered intact following a 20 h incubation (Yamaizumi et al., 1982).

**2.1.2 Model Equations**—Species balances were written for the DT/DTR trafficking pathway based on the model assumptions listed in Section 2.1.1. Note that the model accounts for some spatial dependence by defining separate species based on their locations.

Species balance for bulk extracellular DT

$$\frac{d(DT_{bulk})}{dt} = (-k_{DT} DT_{bulk} DTR_{surf} + k_{DT,r} DT - DTR_{surf}) \frac{n_{cell}}{V_{bulk} N_A} \quad (2.1.1)$$

Species balance for surface DTR

$$\begin{aligned} \frac{d(DTR_{surf})}{dt} &= -k_{int,DT} DTR_{surf} - k_{DT} DT_{bulk} DTR_{surf} \\ &+ k_{DT,r} DT - DTR_{surf} \\ &+ k_{deg} DT - DTR_{lys} \\ &+ k_{deg} DTR_{lys} + k_{deg} DTB - DTR_{lys} \end{aligned} \quad (2.1.2)$$

Species balance for surface DT/DTR complex

$$\frac{d(DT - DTR_{surf})}{dt} = k_{DT} DT_{bulk} DTR_{surf} - k_{DT,r} DT - DTR_{surf} - k_{int,DT} DT - DTR_{surf} \quad (2.1.3)$$

Species balance for endosomal DTR

$$\frac{d(DTR_{en})}{dt} = k_{int,DT} DTR_{surf} - k_{lys} DTR_{en} \quad (2.1.4)$$

Species balance for endosomal DT/DTR complex

$$\frac{d(DT - DTR_{en})}{dt} = k_{int,DT} DT - DTR_{surf} - k_{trans} f_{DT} DT - DTR_{en} - k_{lys} (1 - f_{DT}) DT - DTR_{en} \quad (2.1.5)$$

Species balance for endosomal DTB/DTR complex

$$\frac{d(DTB - DTR_{en})}{dt} = k_{trans} f_{DT} DT - DTR_{en} - k_{lys} DTB - DTR_{en} \quad (2.1.6)$$

Species balance for lysosomal DTR

$$\frac{d(DTR_{lys})}{dt} = k_{lys} DTR_{en} - k_{deg} DTR_{lys} \quad (2.1.7)$$

Species balance for lysosomal DT/DTR complex

$$\frac{d(DT - DTR_{lys})}{dt} = k_{lys}(1 - f_{DT}) DT - DTR_{en} - k_{deg} DT - DTR_{lys} \quad (2.1.8)$$

Species balance for lysosomal DTB/DTR complex

$$\frac{d(DTB - DTR_{lys})}{dt} = k_{lys} DTB - DTR_{en} - k_{deg} DTB - DTR_{lys} \quad (2.1.9)$$

Species balance for cytosolic DTA

$$\frac{d(DTA_{cyt})}{dt} = k_{trns} f_{DT} DT - DTR_{en} \quad (2.1.10)$$

**2.1.3 Model Parameters**—While  $k_{int,DT}$  was estimated directly from empirical data found in the literature, other parameters (*i.e.*,  $k_{DT}$ ,  $k_{DT,r}$ ,  $k_{trans}$ ,  $k_{lys}$ ,  $k_{deg}$ ) were estimated by fitting our model equations to experimental data found in the literature using least squares minimization. The following paragraphs will discuss how the model parameter values were determined. A full list of model parameters can be found in Table 1.

The internalization rate constant  $k_{int,DT}$  for DTR and the DT/DTR complex was determined from studies performed by Leppla and colleagues on Vero monkey kidney cells (Dorland et al., 1979). Vero cells are highly sensitive to diphtheria toxin, and have been demonstrated to express between  $1 \times 10^5$  and  $2 \times 10^5$  receptors for DT (Middlebrook et al., 1978). Vero cells were pre-bound at 4°C with  $^{125}\text{I}$ -labeled DT at a concentration (0.3 µg/mL) that was shown to bind between  $1 \times 10^4$  and  $2 \times 10^4$  surface receptor sites. At this time, the cells were washed to remove any unbound toxin, and the cells were incubated at 37°C in fresh media to initiate cell surface DT/DTR complex internalization. Though some of the receptor-bound DT was found to dissociate from its receptor, this effect was negligible. These conditions allowed Eq. (2.1.3) to be simplified to:

$$\frac{d(DT - DTR_{surf})}{dt} = -k_{int,DT} DT - DTR_{surf} \quad (2.1.11)$$

Equation (2.1.11) was then integrated. Applying the initial condition that the total number of DT/DTR complexes at  $t = 0$  is  $DT\_DTR_{surf,0}$  yields:

$$\ln(DT - DTR_{surf}) = -k_{int,DT}t + \ln(DT - DTR_{surf,0}) \quad (2.1.12)$$

Given the half-time ( $t = t_{1/2}$ ) of DT/DTR complex internalization to be 25 min (Dorland et al., 1979), where  $DT - DTR_{surf}$  is equal to  $1/2 DT - DTR_{surf,0}$ , we estimated  $k_{int,DT}$  to be  $0.028 \text{ min}^{-1}$ .

The rate constants  $k_{DT}$ ,  $k_{DT,r}$ ,  $k_{trans}$ ,  $k_{lys}$ , and  $k_{deg}$  were estimated by fitting them using our model equations and the experimental data for cell-mediated DT reduction, as determined by Montecucco and colleagues (Papini et al., 1993), using least squares minimization. In this fitting procedure, we first converted the given percentage data to units of molecules/cell. Similar to the Leppla and colleagues study on Vero cell DT internalization (Dorland et al., 1979), Montecucco and colleagues began their investigation with Vero cells pre-bound with  $^{125}\text{I}$ -labeled DT. To attain equilibrium binding, Vero cells were pre-bound with DT by incubating them for 18 h with  $3 \times 10^{-9} \text{ M}$  ( $DT_0$ ) of  $^{125}\text{I}$ -labeled DT at  $4^\circ\text{C}$ , which inhibits internalization. With this information, we determined the equilibrium number of cell surface DT/DTR complexes ( $DT - DTR_{eq}$ ), in units of molecules/cell, using the following definition of  $K_D$ :

$$K_D \equiv \frac{DT_{eq} DTR_{eq}}{DT - DTR_{eq}} \quad (2.1.13)$$

Here,  $DT_{eq}$  is the equilibrium molar concentration of unbound DT,  $DTR_{eq}$  is the equilibrium number of cell surface receptors in units of molecules/cell, and  $DT - DTR_{eq}$  is the equilibrium number of cell surface complexes in units of molecules/cell. Assuming the total number of receptors ( $DTR_T$ ) does not change during this process, we can rewrite  $DTR_{eq}$  as:

$$DTR_{eq} = DTR_T - DT - DTR_{eq} \quad (2.1.14)$$

Additionally, following appropriate unit conversion,  $DT_{eq}$  can be shown to be equal to:

$$DT_{eq} = DT_0 - \frac{DT - DTR_{eq} n_{cell}}{N_A V_{bulk}} \quad (2.1.15)$$

Substituting Eqs. (2.1.14) and (2.1.15) into (2.1.13) and simplifying, we obtain the following expression:

$$\frac{n_{cell}}{N_A V_{bulk}} (DT - DTR_{eq})^2 - \left( K_D + \frac{n_{cell}}{N_A V_{bulk}} (DTR_T) + (DT_0) \right) (DT - DTR_{eq}) + (DTR_T)(DT_0) = 0 \quad (2.1.16)$$

The quadratic equation was used to solve for  $DT\_DTR_{eq}$ . A  $DTR_T$  value of  $1.5 \times 10^5$  molecules/cell and a  $DT_0$  value of  $3 \times 10^{-9}$  M were used. For  $n_{cell}$ ,  $V_{bulk}$ , and  $N_A$ , the values given in Table 1 were used in the solution. With regard to  $K_D$ , work by the Mekada laboratory had previously determined its value for the DT/DTR interaction to range from 0.7 to  $3 \times 10^{-9}$  M (Iwamoto et al., 1994; Mitamura et al., 1995). As a first approximation for the model, the  $K_D$  value of the DT/DTR interaction was estimated to be  $10^{-9}$  M. With these numbers, we evaluated the following:

$$DT\_DTR_{eq} = \begin{cases} 2.57 \times 10^6 \\ \text{or} \\ 1.11 \times 10^5 \end{cases} \text{ molecules/cell} \quad (2.1.17)$$

However, since the larger value of  $DT\_DTR_{eq}$  ( $2.57 \times 10^6$ ) obtained was greater than  $DTR_T$ , this value was clearly not the solution. Therefore, the initial value of DT/DTR complexes on the cell surface in the Montecucco study was estimated as  $1.11 \times 10^5$  molecules/cell. This initial value of the number of DT/DTR complexes on the cell surface corresponded to approximately the total number of cell-surface DT receptors, which was used to convert the percentage data in the Montecucco study to units of molecules/cell. The conversions were made specifically for the data performed at 37°C investigating the percent  $^{125}\text{I}$ -DT released in the medium and associated with cells and the percent  $^{125}\text{I}$ -DTA associated with cells. The data was then used to fit the  $k_{DT}$ ,  $k_{DT,r}$ ,  $k_{trans}$ ,  $k_{lys}$ , and  $k_{deg}$  rate constants by using the DT/DTR trafficking model equations and least squares minimization with initial conditions set to zero for all species except  $DT\_DTR_{surf}$  ( $1.11 \times 10^5$  molecules/cell), and  $DTR_{surf}$  ( $3.92 \times 10^4$  molecules/cell). The model fit the experimental data reasonably well. Estimates for the  $k_{DT}$ ,  $k_{DT,r}$ ,  $k_{trans}$ ,  $k_{lys}$ , and  $k_{deg}$  rate constants were determined to be  $1.90 \times 10^7 \text{ M}^{-1} \text{ min}^{-1}$ ,  $1.90 \times 10^{-2} \text{ min}^{-1}$ ,  $1.5 \times 10^{-1} \text{ min}^{-1}$ ,  $1.8 \times 10^{-1} \text{ min}^{-1}$ , and  $4.0 \times 10^{-2} \text{ min}^{-1}$ , respectively. The fitted parameters  $k_{DT}$ ,  $k_{DT,r}$ ,  $k_{lys}$ , and  $k_{deg}$  were reasonably similar to literature values of comparable biomolecules (Gallegos et al., 2012; French and Lauffenburger, 1997).

With regard to the association rate constant of DT for DTR,  $k_{DT}$ , it was estimated by the following equality for the equilibrium dissociation constant ( $K_D$ ):

$$K_D = \frac{k_{DT,r}}{k_{DT}} \quad (2.1.18)$$

In this estimation, the  $K_D$  value of the DT/DTR interaction was again estimated to be  $10^{-9}$  M, and  $k_{DT,r}$  was estimated in the above fitting procedure to be  $1.90 \times 10^{-2} \text{ min}^{-1}$ .

## 2.2 Mathematical model of mutant Tf-DT conjugate intracellular trafficking

To fully model the Tf-toxin conjugates, we combined our Tf/TfR model developed previously (Lao et al., 2007) with the DT/DTR trafficking model developed in Section 2.1. The model assumptions are discussed in this section, as are the relevant equations and parameters.

**2.2.1 Model Assumptions**—The model assumptions used for the development of the Tf/TfR (Lao et al., 2007) and DT/DTR (Section 2.1) trafficking models also apply to the Tf-DT trafficking model with the following changes and additions.

- i. Direct measurements of the iron release rate within cellular endosomes,  $k_{Fe,rel}$  are unavailable for both wild-type and mutant Tf. However, since iron is completely released from internalized wild-type Tf prior to recycling back to the cell surface (Ciechanover et al., 1983), the same estimate of  $100 \text{ min}^{-1}$  as used in the Tf/TfR trafficking model was applied to the Tf-DT conjugate trafficking model for wild-type Tf-DT.
- ii. Since  $k_{Fe,rel}$  for our mutant Tf had previously been estimated to be on the order of  $10^{-3} \text{ min}^{-1}$  (Halbrooks et al., 2003), this value was assumed in the model for mutant Tf-DT conjugates.
- iii. Since the binding affinity of CRM107 to preHB-EGF is 8,000-fold less than that of DT to preHB-EGF,  $k_{DT}$  was lowered by 8,000-fold for CRM107 conjugates.
- iv. The vesicle/tubule partition coefficient,  $\kappa$ , was calculated according to the expression  $\kappa = (1-\lambda)^2$ , where  $\lambda$  is the diameter of the Tf-DT conjugate divided by the diameter of the tubule (French and Lauffenburger, 1996). An average Tf-DT conjugate diameter of 20 nm was estimated from the crystal structures of Tf (Kilar and Simon, 1985) and DT (Choe et al., 1992) by summing the longest length scale of each individual molecule together. A tubule diameter of 60 nm was assumed (Marsh et al., 1986).
- v. Endosomal Tf-DT conjugates, not associated with either receptor, were assumed to be unable to associate with the endosomal membrane and translocate DTA.
- vi. It was assumed that the Tf-DT conjugate was required to be associated with TfR in the vesicular compartment (which is destined for degradation) to be competent for DTA translocation into the cytosol when internalized via the Tf/TfR trafficking pathway. This is supported by studies demonstrating that DT membrane insertion and translocation requires an endosomal pH drop to  $\sim 4$  (Chenal et al., 2009), while endosomal pH is not expected to drop below  $\sim 5.5$  in the Tf/TfR recycling pathway (Dautry-Varsat et al., 1983; Klausner et al., 1983a).
- vii. It was assumed that once the DT portion of the conjugate had associated with the endosomal membrane and translocated its catalytic domain into the cytosol, the remaining endosomal molecule was sorted for lysosomal degradation through the DT/DTR trafficking pathway irrespective of the receptor the conjugate was associated with.

**2.2.2 Model Equations**—The full list of all species balances associated with the Tf-DT conjugate intracellular trafficking model can be found in the Supplementary Information. A short description of each species is given prior to each species balance expression. Note that, as before, species are defined based on their type and location in order to recognize the spatial differences in the trafficking pathway. To clarify, any species referred to as “reduced”

(e.g., reduced FeTfDT/TfR complex and reduced TfDT/DTR complex) signifies that the disulfide bond between the DTA and DTB domains of DT has been cleaved through the process defined by the rate constant  $k_{trans}$ . Therefore, reduced versions of the Tf-DT conjugates (i.e., FeTfDT and TfDT) are represented in the species balances as FeTfDTB and TfDTB. The rate constant,  $k_{trans}$ , also captures the process by which DTA translocates into the cytosol following this disulfide reduction.

**2.2.3 Model Parameters**—Mutant Tf conjugates were differentiated from wild-type Tf conjugates by altering the iron release rate within cellular endosomes,  $k_{Fe,rel}$ , such that mutant Tf conjugates had a lower  $k_{Fe,rel}$ . CRM107 conjugates were differentiated from DT conjugates by altering the binding affinity to DTR. CRM107's decreased binding affinity for DTR was modeled by setting the DT to DTR association rate constant,  $k_{DT}$ , of Tf-CRM107 simulations to be 8,000-fold less than its value for Tf-DT simulations. Note that this same distinction between Tf-DT and Tf-CRM107 conjugates can also be accomplished by increasing the DT to DTR dissociation rate constant,  $k_{DT,r}$ , by 8,000-fold for Tf-CRM107 simulations since  $K_D = k_{DT,r}/k_{DT}$ . It was found with the cellular toxicity simulations that either method produced the same outcome. The results in Section 3 correspond to decreasing the association rate constant for Tf-CRM107 conjugates. In addition, the same rate constant for TfR-mediated internalization was assumed for both Tf and its mutant. This was deduced from the fact that the TfR-mediated internalization rate constant remains the same regardless of whether there is Tf bound to TfR (Watts, 1985), which suggests that the internalization rate constant would not depend on the type of Tf bound to TfR. A full list of model parameters is provided in Table 2.

## 2.3 *In Silico* Cytotoxicity

**2.3.1 Cellular Toxicity in Cancerous Cells**—Model equations were solved with Berkeley Madonna™ using initial conditions set to zero for all species except the concentration of holo-Tf-DT (1 nM), the number of TfR on the cell surface ( $5.4 \times 10^5$  receptors; Yazdi and Murphy, 1994), and the number of DTR on the cell surface ( $1.5 \times 10^5$  receptors; Middlebrook et al., 1978). The length of each simulation was 50 h. Wild-type Tf conjugates were distinguished from mutant Tf conjugates by setting the endosomal iron release rate constant,  $k_{Fe,rel}$ , to  $100 \text{ min}^{-1}$  and  $0.001 \text{ min}^{-1}$ , respectively. Tf-CRM107 conjugate trafficking was distinguished from Tf-DT conjugate trafficking by reducing the association rate constant for toxin binding to DTR ( $k_{DT}$ ) to be 8,000-fold less.

Cellular toxicity was investigated by examining the % inhibition of cellular growth at various concentrations of the Tf-toxin conjugate. Tf-toxin conjugate-induced cellular toxicity was estimated using the following approach. First, based on our previous Tf-DT conjugate *in vitro* toxicity studies with U251 and U87 cells, maximum wild-type Tf-DT toxicity initially plateaued at a conjugate concentration of  $3.16 \times 10^{-11} \text{ M}$  for both cell lines (Yoon et al., 2010). The number of molecules of DT's catalytic domain (DTA) found in the cytosol at this concentration was determined from trafficking simulations to be  $1.51 \times 10^4$  molecules/cell, and this was fixed as the number of DTA molecules necessary to exhibit 100% cellular toxicity for our model simulations. Lower concentrations of conjugates were also input into the trafficking model to generate a cytotoxicity curve. After determining the

number of DTA molecules in the cytosol, the value was divided by  $1.51 \times 10^4$  and multiplied by 100% to yield the corresponding % inhibition value.

**2.3.2 Cellular Toxicity in Non-Neoplastic Cells**—Cellular toxicity for non-neoplastic cells was investigated similarly to the procedure outlined in Section 2.3.1, with the exception of the initial value of surface Tf receptors. Since cancerous cells are known to overexpress surface TfR (Daniels et al., 2006), non-neoplastic cells were modeled by decreasing the initial surface TfR of cancerous cells,  $5.4 \times 10^5$  receptors (Yazdi and Murphy, 1994), by various fold. Since non-neoplastic cells were expected to have at least 10-fold fewer TfR than cancerous cells, this investigation was started at a 10-fold decrease of TfR.

## 2.4 *In Vitro* Cytotoxicity

Tf-toxin conjugates were synthesized and various cell lines were cultured according to methods detailed in Sections 1 and 2 of the Supplementary Information. The sulforhodamine B (SRB) cell proliferation assay was used to quantify cell survival based on the measurement of cellular protein content. The toxicities of the mutant Tf-CRM107 conjugates relative to the wild-type Tf-CRM107 conjugate were investigated in glioma cells (U87 and U251) and HeLa cells to determine if the mutant Tf conjugates were more potent than the wild-type Tf conjugate using the new toxin. In addition, mutant Tf-CRM107 conjugates were incubated with normal cells to assess cancer specificity.

The various cells utilized in this study were seeded onto wells of a 96-well tissue culture plate at cell densities of 10,000 cells/cm<sup>2</sup> for cancer cells (U87, U251, and HeLa) and 45,000 cells/cm<sup>2</sup> for normal cells (human umbilical vein endothelial cell (HUVEC) and normal human astrocyte (NHA)). Different seeding densities were used due to differences in cell size and proliferation rate. Following overnight incubation, growth medium was aspirated, and the cells were incubated for 48 h with 100  $\mu$ L fresh growth medium containing concentrations of Tf-CRM107 spanning five orders of magnitude ( $10^{-13}$  to  $10^{-9}$  M). A cold 10% trichloroacetic acid (TCA) solution (100  $\mu$ L) was added to each well to fix the cells at 4°C for 1 h. The 10% TCA solution was removed, and the cells were washed four times with deionized water then thoroughly blow-dried. Subsequently, 50  $\mu$ L of a 1% acetic acid solution containing 0.4% SRB was added to each well for 30 min at room temperature. The dye solution was removed, and the cells were washed four times with a 1% acetic acid solution to remove unbound dye; following this step, the cells were again blow-dried. The dye was dissociated from the proteins and solubilized with 100  $\mu$ L of a 10 mM Tris base solution. The absorbance of each well was determined with an Infinite F200 plate reader (Tecan System Inc., San Jose, CA) at wavelengths of 560 and 700 nm. The survival of cells relative to a control (*i.e.*, cells incubated in growth medium without Tf-CRM107) was calculated by determining the ratio of the ( $A_{560} - A_{700}$ ) values. Experiments were performed three times with quadruplicate points per concentration.

### 3 Results and Discussion

#### 3.1 Tf-DT Mathematical Model Successfully Predicts Improved Efficacy of Mutant Tf-CRM107 Conjugates against Cancer Cells Relative to Wild-Type Tf-CRM107 Conjugates

Simulations with our Tf-DT conjugate intracellular trafficking model were performed to determine differences in cytotoxicity between wild-type and mutant Tf proteins with both DT and CRM107 conjugates. The predicted trends were then validated with *in vitro* cytotoxicity data.

Figure 3 and Table 3 presents the results of our *in silico* toxicity simulations. The concentrations at which 50% inhibition of cellular growth ( $IC_{50}$ ) was observed were 13.4, 8.66, 36.8, and 8.20 pM for wild-type Tf-DT, mutant Tf-DT, wild-type Tf-CRM107, and mutant Tf-CRM107, respectively (Table 3). These results indicate that mutant Tf conjugates have increased drug efficacy compared to the wild-type conjugates. In addition, the difference in drug delivery efficacy between wild-type and mutant Tf was only 1.5-fold for DT conjugates, while the difference for CRM107 conjugates was 4.5-fold. This suggests that changing the toxin moiety of our Tf-based cancer therapeutic from DT to CRM107 can potentially increase the difference in drug efficacy. A sensitivity analysis was performed (Section 6 in the Supporting Information) to verify that the trends presented in this modeling results section were maintained for a wide range of values for key parameters in the model.

The difference in cytotoxicity between CRM107 and DT was as predicted because the wild-type Tf-CRM107 conjugate was estimated to be associated to a lesser degree with the cell than the wild-type Tf-DT conjugate, since CRM107 cannot bind to DTR (the preHB-EGF receptor). Wild-type Tf is often assumed to be restricted to a single cycle through its trafficking pathway due to its highly efficient iron delivery kinetics (Ciechanover et al., 1983; Yazdi and Murphy, 1994). For this reason, wild-type Tf-CRM107 conjugates would typically have a single opportunity to deliver their cytotoxic payload, which is insufficient for the effective delivery of CRM107 given the short intracellular residence time of a single Tf/TfR trafficking cycle (Klausner et al., 1983b). On the other hand, wild-type Tf-DT conjugates are given an additional opportunity to deliver their cytotoxic payload even after the loss of iron because of DT's high affinity for its own receptor. Coupled with the greater intracellular residence time associated with the DT/DTR degradation pathway (Dorland et al., 1979), it is not surprising that the cytotoxicity of wild-type Tf-DT conjugates is significantly greater than the cytotoxicity of wild-type Tf-CRM107 conjugates.

To confirm these trends predicted by the Tf-DT conjugate intracellular trafficking and toxicity model, we synthesized and administered CRM107 conjugates of our wild-type, K206E/R632A, and K206E/K534A Tf ligands to two glioma (U251 and U87) cell lines as well as the HeLa cell line over a range of concentrations for 48 h. In accordance with our model, each mutant Tf-CRM107 conjugate exhibited a significantly enhanced drug delivery efficacy relative to their wild-type counterpart in U87, U251, and HeLa cells that was much greater than the improved efficacy observed with Tf-DT conjugates (Figure 4, Table 4).  $IC_{50}$  values for U87 cells (Figures 4A and B, Table 4) were determined to be  $32.1 \pm 3.2$  pM for wild-type Tf compared to values of  $7.10 \pm 0.87$  ( $p = 0.0002$ ) and  $6.80 \pm 0.52$  pM ( $p = 0.0002$ ) for K206E/R632A Tf and K206E/K534A Tf, respectively. Similar results were

obtained with U251 cells (Figures 4C and D, Table 4), demonstrating  $IC_{50}$  values of  $35.3 \pm 3.7$  pM for wild-type Tf compared to values of  $10.8 \pm 1.8$  ( $p = 0.0005$ ) and  $11.3 \pm 1.2$  pM ( $p = 0.0004$ ) for K206E/R632A Tf and K206E/K534A Tf, respectively. For HeLa cells (Figures 4E and F, Table 4), the  $IC_{50}$  values were determined to be  $30.3 \pm 3.0$  pM for wild-type Tf compared to values of  $9.4 \pm 1.0$  ( $p = 0.0002$ ) and  $10.2 \pm 1.4$  pM ( $p = 0.0003$ ) for K206E/R632A Tf and K206E/K534A Tf, respectively. The student's *t*-test was used to show that the decrease in  $IC_{50}$  exhibited by both mutant Tf-CRM107 conjugates compared to the wild-type counterpart was statistically significant ( $p < 0.05$ ). These experiments showed that mutant Tf-CRM107 conjugates exhibited an improved efficacy compared to wild-type Tf-CRM107 conjugates (4.6, 3.2, and 3.0 fold for U87, U251, and HeLa cells). The fold improvement observed with the mutant Tf-CRM107 conjugates relative to the wild-type Tf-CRM107 conjugate was greater than the fold improvement observed with the mutant Tf-DT conjugates relative to the wild-type Tf-DT conjugate (Yoon et al., 2009, 2010).

These *in vitro* results are consistent with our projected trends that mutant Tf conjugates have an improved efficacy compared to wild-type Tf conjugates. Our mathematical model of the Tf-DT intracellular trafficking pathway thus successfully predicted that (i) mutant Tf-toxin conjugates were more effective than wild-type Tf-toxin conjugates, and (ii) the increase in drug carrier efficacy for CRM107 conjugates was better than for DT conjugates. These results suggest that CRM107 appears to be a more suitable therapeutic agent for our mutant Tf to deliver to cancer cells.

### 3.2 Tf-DT Mathematical Model Successfully Predicts Selectivity of Mutant Tf-CRM107 for Cancerous Cells Relative to Non-Neoplastic Cells

Simulations with our Tf-DT conjugate intracellular trafficking model were performed to determine differences in selectivity of the mutant Tf-CRM107 conjugate for cancerous, or neoplastic, cells relative to non-neoplastic cells. The predicted trends were then validated with *in vitro* cytotoxicity data.

To simulate the cancer selectivity of our mutant Tf-CRM107 conjugates, we also ran cellular toxicity simulations with varying numbers of TfR receptors. Since TfR is overexpressed on malignant cells at  $5.4 \times 10^5$  receptors on the cell surface (Daniels et al., 2006; Yazdi and Murphy, 1994), we varied the number of initial TfR receptors over a range of decreased values to model non-neoplastic cells. The results can be found below in Figure 5. The simulated  $IC_{50}$  values of mutant Tf-CRM107 in neoplastic cells was 8.20 pM, while the simulated values for non-neoplastic cells were 11.5 pM, 16.4 pM, 81.0 pM, and 144.4 pM for  $5.4 \times 10^4$ ,  $2.97 \times 10^4$ ,  $5.4 \times 10^3$ , and  $2.97 \times 10^3$  TfR, respectively (Table 5). The results from this *in silico* study shows the trend that decreasing numbers of TfR (*i.e.*, modeling non-neoplastic cells) results in reduced cytotoxicity of our mutant Tf-CRM107 conjugates. Our model thus predicts that mutant Tf-CRM107 conjugates demonstrate selectivity for cancerous cells relative to non-neoplastic cells, and suggests that they could be used as a targeted cancer therapeutic agent.

These differences between cancerous and non-neoplastic cells were predicted for mutant Tf-CRM107 because the conjugates are estimated to associate to a lesser degree with cells that have fewer TfR on the surface. Since the binding affinity of CRM107 for DTR is 8,000-fold

lower than native values and the binding affinity of mutant Tf to TfR remains the same compared to native values (Yoon et al., 2009), the main contribution to internalization of the mutant Tf-CRM107 conjugates is the Tf/TfR pathway. The decreased numbers of TfR on cell surfaces of non-neoplastic cells thus results in decreased mutant Tf-CRM107 internalization. Because of this difference in conjugate internalization for neoplastic versus non-neoplastic cells, the conjugates were less cytotoxic toward and selective against non-neoplastic cells.

To validate our cytotoxicity simulations of the mutant Tf-CRM107 conjugates in non-neoplastic cells, *in vitro* cytotoxicity experiments were performed with two non-neoplastic cell types, HUVECs and NHAs. Our results indicated that cancer selectivity can be achieved by our CRM107 conjugates due to significantly higher  $IC_{50}$  values observed for all conjugates when treating non-neoplastic cells, suggesting a potentially good therapeutic index. As seen in Figures 6A and B,  $IC_{50}$  values for HUVECs were determined to be  $195 \pm 30$ ,  $147 \pm 36$  ( $p = 0.2$ ), and  $136 \pm 24$  pM ( $p = 0.06$ ) for wild-type Tf, K206E/R632A Tf, and K206E/K534A Tf, respectively. Similar results were obtained with NHAs (Figures 6C and D), demonstrating  $IC_{50}$  values of  $55.0 \pm 9.3$ ,  $32.4 \pm 7.4$  ( $p = 0.03$ ), and  $38.0 \pm 6.8$  pM ( $p = 0.06$ ) for wild-type Tf, K206E/R632A Tf, and K206E/K534A Tf, respectively. Compared to the *in vitro*  $IC_{50}$  values for cancerous cells presented in Section 3.1, these values are much higher, confirming our mathematical prediction that our mutant Tf-CRM107 conjugates exhibit selectivity for cancerous cells relative to non-neoplastic cells. From these results, we can conclude that changing the toxin moiety from DT to CRM107, which has an 8,000-fold reduced binding affinity, has a significant contribution to improving the selectivity.

In addition, differences in toxicity between wild-type Tf-CRM107 conjugates and both mutant Tf-CRM107 conjugates were significantly diminished in non-neoplastic cell lines. The student's *t*-test was used to show that the decrease in  $IC_{50}$  exhibited by both mutant Tf-CRM107 conjugates compared to the wild-type counterpart was not statistically significant ( $p > 0.05$ ), with the exception of the K206E/R632A Tf-CRM107 conjugate against NHAs. The diminished difference in  $IC_{50}$  values was likely due to saturation of TfR with the conjugates. Since normal cells are expected to express far fewer TfR, additional recycling capabilities of the mutant conjugates become inconsequential in the presence of excess Tf-CRM107 conjugates available to bind to the receptors and be internalized.

## 4 Conclusion

Due to the overexpression of TfR on cancer cells, targeted cancer therapeutics that exploit the Tf trafficking pathway is currently being evaluated. Previously, we have used a mathematical model of the Tf/TfR pathway to predict that conjugates made with a mutated form of Tf results in improved efficacy in cancer cell lines. Though we have previously investigated mutant Tf-DT conjugates with success, DT has high toxicity and may exhibit dangerous off-target effects.

In this work, we proposed the utilization of a mathematical model to evaluate the efficacy and selectivity of mutant Tf conjugated to an alternate drug. For this mathematical investigation of a novel conjugate, we chose to investigate CRM107, a mutant form of DT.

We first extended our previously developed Tf/TfR model to include a DT/DTR pathway. We then used our mathematical model to evaluate how mutant Tf would improve efficacy compared to wild-type Tf when the toxin moiety is changed to CRM107 and whether a mutant Tf-CRM107 conjugate would exhibit improved selectivity against non-neoplastic cells while maintaining cytotoxic efficacy toward cancerous cells.

Through our simulations, we predicted that mutant Tf-CRM107 would outperform wild-type Tf-CRM107 in terms of efficacy toward cancer cells. We also predicted that switching from wild-type Tf to mutant Tf in CRM107 conjugates would drastically improve the efficacy of these conjugates due to the absence of the DT/DTR trafficking pathway for CRM107. In addition, this increase was predicted to be much greater than the increase associated with switching from wild-type Tf to mutant Tf in DT conjugates. This predicted trend was confirmed in our *in vitro* investigation of toxicity with the U87 and U251 glioma cell lines, as well as the HeLa cell line.

We also ran simulations to evaluate the selectivity of this novel mutant Tf-CRM107 conjugate. The results of our simulation suggested that the cytotoxicity of mutant Tf-CRM107 was greater in cancerous cells due to overexpression of TfR on those cells. This predicted trend was confirmed, as our measured *in vitro* IC<sub>50</sub> values of CRM107 conjugates with normal cell lines were many fold higher than the IC<sub>50</sub> values observed with cancerous cell lines. Both our *in silico* simulations and *in vitro* results suggest a potentially greater therapeutic window for the mutant Tf-CRM107 conjugates. Furthermore, for the normal cell types (HUVECs and NHAs), the cytotoxicity curves of the mutant and wild-type Tf-CRM107 conjugates became similar, attributed to the saturation of TfR on the normal cells.

In summary, our mathematical model predicted that (i) mutant Tf-CRM107 exhibited improved efficacy compared to wild-type Tf-CRM107, (ii) this improvement in efficacy was greater than that of its DT counterparts, and (iii) mutant Tf-CRM107 exhibits a substantial decrease in toxic side effects. These mathematical simulations, which were validated by our *in vitro* studies, altogether indicate that CRM107 would be a more suitable therapeutic agent in combination with the mutant Tf in future studies.

## Supplementary Material

Refer to Web version on PubMed Central for supplementary material.

## Acknowledgments

This work was funded by the Wallace H. Coulter Foundation Early Career Award (D.T. Kamei), the Cancer Research Coordinating Committee grant (D.T. Kamei), the USPHS grant R01 DK 21739 (A.B. Mason), and the National Council for Scientific and Technological Development CNPq/Brazil #234339/2014-4 (A.M. Lopes). The authors thank Drs. Robert M. Prins and Linda M. Liao, Department of Neurosurgery, UCLA, for kindly providing the U251 cells.

## References

Cazzola M, Bergamaschi G, Dezza L, Arosio P. Manipulations of cellular iron metabolism for modulating normal and malignant cell proliferation: achievements and prospects. *Blood*. 1990; 75:1903–1919. [PubMed: 2186818]

- Chenal A, Prongidi-Fix L, Perier A, Aisenbrey C, Vernier G, Lambotte S, Fragneto G, Bechinger B, Gillet D, Forge V, Ferrand M. Deciphering membrane insertion of the diphtheria toxin T domain by specular neutron reflectometry and solid-state NMR spectroscopy. *J Mol Biol.* 2009; 391:872–883. [PubMed: 19576225]
- Choe S, Bennett MJ, Fujii G, Curmi PM, Kantardjieff KA, Collier RJ, Eisenberg D. The crystal structure of diphtheria toxin. *Nature.* 1992; 357:216–222. [PubMed: 1589020]
- Ciechanover A, Schwartz AL, Dautry-Varsat A, Lodish HF. Kinetics of internalization and recycling of transferrin and the transferrin receptor in a human hepatoma cell line. Effect of lysosomotropic agents. *J Biol Chem.* 1983; 258:9681–9689. [PubMed: 6309781]
- Collier RJ. Diphtheria toxin: mode of action and structure. *Bacteriol Rev.* 1975; 39:54–85. [PubMed: 164179]
- Daniels TR, Delgado T, Helguera G, Penichet ML. The transferrin receptor part II: Targeted delivery of therapeutic agents into cancer cells. *Clinical Immunology.* 2006; 121:159–176. [PubMed: 16920030]
- Dautry-Varsat A, Ciechanover A, Lodish HF. pH and the recycling of transferrin during receptor-mediated endocytosis. *P Natl Acad Sci USA.* 1983; 80:2258–2262.
- Dorland RB, Middlebrook JL, Leppla SH. Receptor-mediated internalization and degradation of diphtheria toxin by monkey kidney cells. *J Biol Chem.* 1979; 254:11337–11342. [PubMed: 115867]
- French AR, Lauffenburger DA. Intracellular receptor/ligand sorting based on endosomal retention components. *Biotechnol Bioeng.* 1996; 51:281–297. [PubMed: 18624361]
- French AR, Lauffenburger DA. Controlling receptor/ligand trafficking: effects of cellular and molecular properties on endosomal sorting. *Ann Biomed Eng.* 1997; 25:690–707. [PubMed: 9236981]
- Gallegos KM, Conrady DG, Karve SS, Gunasekera TS, Herr AB, Weiss AA. Shiga toxin binding to glycolipids and glycans. *PLoS ONE.* 2012; 7(2)
- Goishi K, Higashiyama S, Klagsbrun M, Nakano N, Umata T, Ishikawa M, Mekada E, Taniguchi N. Phorbol ester induces the rapid processing of cell surface heparin-binding EGF-like growth factor: conversion from juxtacrine to paracrine growth factor activity. *Mol Biol Cell.* 1995; 6:967–980. [PubMed: 7579712]
- Halbrooks PJ, He QY, Briggs SK, Everse SJ, Smith VC, MacGillivray RTA, Mason AB. Investigation of the mechanism of iron release from the C-lobe of human serum transferrin: mutational analysis of the role of a pH sensitive triad. *Biochemistry.* 2003; 42:3701–3707. [PubMed: 12667060]
- Iwamoto R, Higashiyama S, Mitamura T, Taniguchi N, Klagsbrun M, Mekada E. Heparin-binding EGF-like growth factor, which acts as the diphtheria toxin receptor, forms a complex with membrane protein DRAP27/CD9, which up-regulates functional receptors and diphtheria toxin sensitivity. *Embo J.* 1994; 13:2322–2330. [PubMed: 8194524]
- Johnson VG, Wilson D, Greenfield L, Youle RJ. The role of the diphtheria toxin receptor in cytosol translocation. *J Biol Chem.* 1988; 263:1295–1300. [PubMed: 3257214]
- Johnson VG, Wrobel C, Wilson D, Zovickian J, Greenfield L, Oldfield EH, Youle R. Improved tumor-specific immunotoxins in the treatment of CNS and leptomeningeal neoplasia. *J Neurosurg.* 1989; 70:240–248. [PubMed: 2783608]
- Kilar F, Simon I. The effect of iron binding on the conformation of transferrin. A small angle x-ray scattering study. *Biophys J.* 1985; 48:799–802. [PubMed: 4074838]
- Klausner RD, Ashwell G, Van Renswoude J, Harford JB, Bridges KR. Binding of apotransferrin to K562 cells: explanation of the transferrin cycle. *P Natl Acad Sci USA.* 1983; 80:2263–2266.
- Klausner RD, Van Renswoude J, Ashwell G, Kempf C, Schechter AN, Dean A, Bridges KR. Receptor-mediated endocytosis of transferrin in K562 cells. *J Biol Chem.* 1983; 258:4715–4724. [PubMed: 6300098]
- Lao BJ, Tsai WL, Mashayekhi F, Pham EA, Mason AB, Kamei DT. Inhibition of transferrin iron release increases *in vitro* drug carrier efficacy. *J Control Release.* 2007; 117:403–412. [PubMed: 17239470]
- Lao BJ, Kamei DT. Improving therapeutic properties of protein drugs through alteration of intracellular trafficking pathways. *Biotechnol Progr.* 2008; 24:2–7.

- Lebron JA, Bennett MJ, Vaughn DE, Chirino AJ, Snow PM, Mintier GA, Feder JN, Bjorkman PJ. Crystal structure of the hemochromatosis protein HFE and characterization of its interaction with transferrin receptor. *Cell*. 1998; 93:111–123. [PubMed: 9546397]
- Marsh M, Griffiths G, Dean GE, Mellman I, Helenius A. Three-dimensional structure of endosomes in BHK-21 cells. *P Natl Acad Sci USA*. 1986; 83:2899–2903.
- Middlebrook JL, Dorland RB, Leppla SH. Association of diphtheria toxin with Vero cells. Demonstration of a receptor. *J Biol Chem*. 1978; 253:7325–7330. [PubMed: 701254]
- Mitamura T, Higashiyama S, Taniguchi N, Klagsbrun M, Mekada E. Diphtheria toxin binds to the epidermal growth factor (EGF)-like domain of human heparin-binding EGF-like growth factor/diphtheria toxin receptor and inhibits specifically its mitogenic activity. *J Biol Chem*. 1995; 270:1015–1019. [PubMed: 7836353]
- Papini E, Rappuoli R, Murgia M, Montecucco C. Cell penetration of diphtheria toxin. Reduction of the interchain disulfide bridge is the rate-limiting step of translocation in the cytosol. *J Biol Chem*. 1993; 268:1567–1574. [PubMed: 8420931]
- Ponka P, Lok CN. The transferrin receptor: role in health and disease. *Int J Biochem Cell Biol*. 1999; 31:1111–1137. [PubMed: 10582342]
- Qian ZM, Li H, Sun H, Ho K. Targeted drug delivery via the transferrin receptor-mediated endocytosis pathway. *Pharmacol Rev*. 2002; 54:561–587. [PubMed: 12429868]
- Ronnberg BJ, Middlebrook JL. Cellular regulation of diphtheria toxin cell surface receptors. *Toxicol*. 1989; 27:1377–1388. [PubMed: 2629178]
- Siegel RL, Miller KD, Jemal A. Cancer statistics, 2016. *Ca Cancer J Clin*. 2016; 66:7–30. [PubMed: 26742998]
- Watts C. Rapid endocytosis of the transferrin receptor in the absence of bound transferrin. *Journal of Cell Biology*. 1985; 100(2):633–637. [PubMed: 2857182]
- Yamaizumi M, Uchida T, Takamatsu K, Okada Y. Intracellular stability of diphtheria toxin fragment A in the presence and absence of anti-fragment A antibody. *P Natl Acad Sci USA*. 1982; 79:461–465.
- Yazdi PT, Murphy RM. Quantitative analysis of protein synthesis inhibition by transferrin–toxin conjugates. *Cancer Res*. 1994; 54:6387–6394. [PubMed: 7987833]
- Yoon DJ, Chu DSH, Ng CW, Pham EA, Mason AB, Hudson DM, Smith VC, MacGillivray RTA, Kamei DT. Genetically engineering transferrin to improve its *in vitro* ability to deliver cytotoxins. *J Control Release*. 2009; 133:178–184. [PubMed: 18992290]
- Yoon DJ, Kwan BH, Chao FC, Nicolaidis TP, Phillips JJ, Lam GY, Mason AB, Weiss WA, Kamei DT. Intratumoral therapy of glioblastoma multiforme using genetically engineered transferrin for drug delivery. *Cancer Res*. 2010; 70:4520–4527. [PubMed: 20460527]

## Appendix A Supplementary Information

Supplementary information associated with this article can be found, in the online version, at [URL].

### Highlights

- Developed mathematical model of Tf-DT intracellular trafficking pathway
- Used model to predict drug efficacy and selectivity of mutant Tf-CRM107 conjugates
- Validated predictions with *in vitro* cytotoxicity experiments
- Mutant Tf-CRM107 exhibits improved efficacy
- Mutant Tf-CRM107 exhibits good therapeutic index for cancer therapy

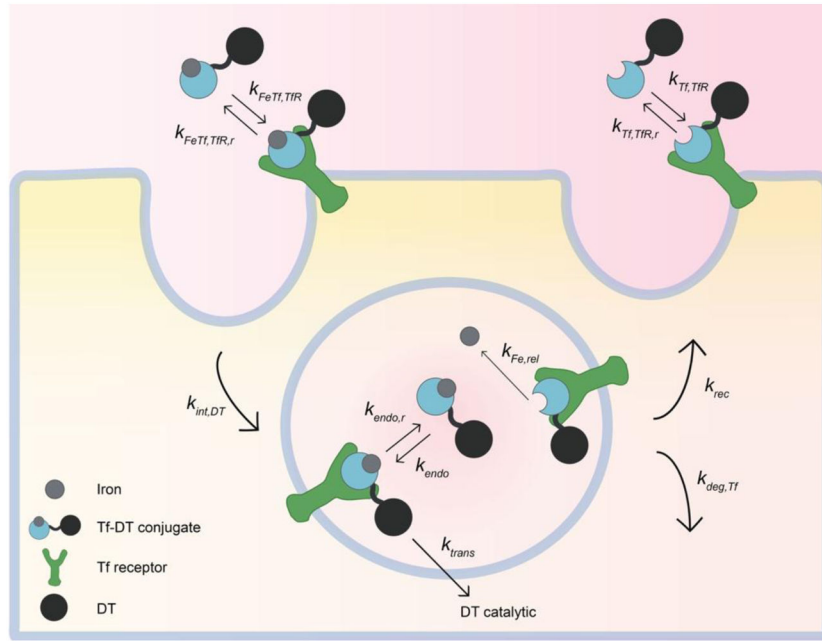


**Fig. 1. Tf-related trafficking parameters used in the combined Tf-DT trafficking pathway**  
 For this part of the pathway, holo-Tf conjugated with DT enters the cell through TfR, then internalized as a holo-Tf/TfR complex. DT can then be cleaved, and DTA is released into the cytosol. After iron from Tf is released, the apo-Tf/TfR complex is either degraded or recycled. For the recycled apo-Tf/TfR complex, the apo-Tf is released when it returns to the cell surface.

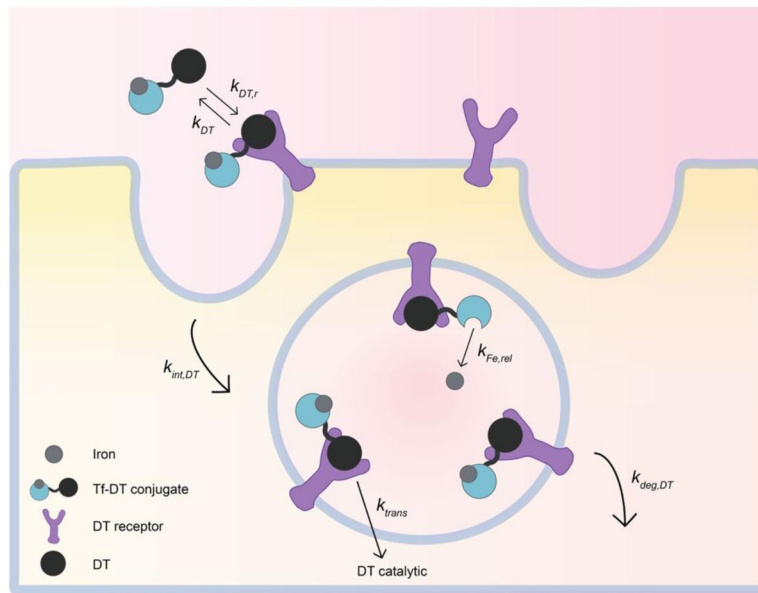


**Fig. 2. DT-related trafficking parameters used in the combined Tf-DT trafficking pathway**  
 For this part of the pathway, Tf-DT conjugates enter the cell through binding to DTR. The Tf-DT/DTR complex is then internalized, where DT can be cleaved and DTA can be translocated into the cytosol. In addition, once inside the cell, iron can be released from Tf, and the Tf-DT/DTR complex can be degraded.

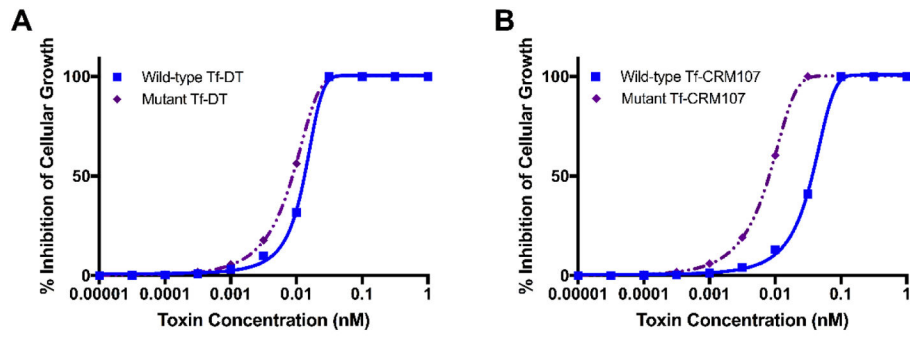


**Figure 3. Cytotoxicity simulation of wild-type Tf versus mutant Tf conjugates**  
*In silico* cytotoxicity simulations using the Tf-DT mathematical model for (A) wild-type and mutant Tf-DT conjugates and (B) wild-type and mutant Tf-CRM107 conjugates.

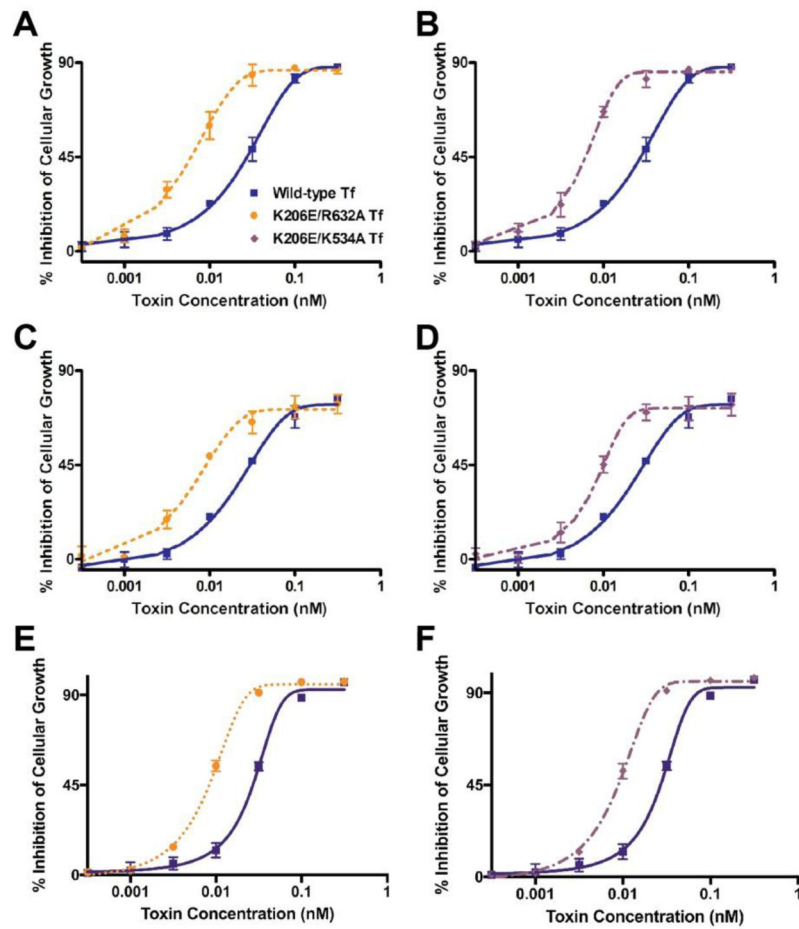


**Figure 4. *In vitro* cytotoxicity comparisons for CRM107 conjugates**

Points, mean from an average of three experiments; bars, standard deviation. Wild-type Tf versus K206E/R632A Tf and K206E/R534A Tf in (A, B) U87, (C, D) U251, and (E, F) HeLa cells.

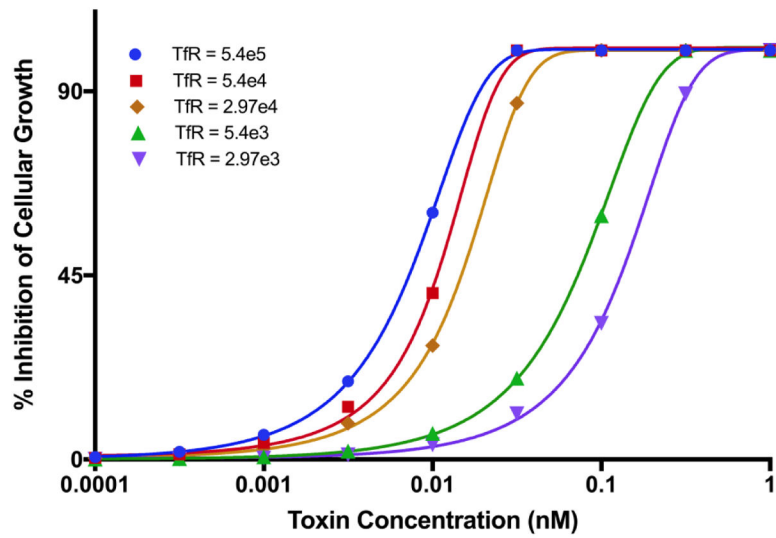


**Figure 5. Cytotoxicity simulation of mutant Tf-CRM107 conjugates against neoplastic and non-neoplastic cells**

Cytotoxicity curves of neoplastic cells ( $TfR = 5.4 \times 10^4$ ) versus non-neoplastic cells show a trend of reduced cytotoxicity with reduced TfR.

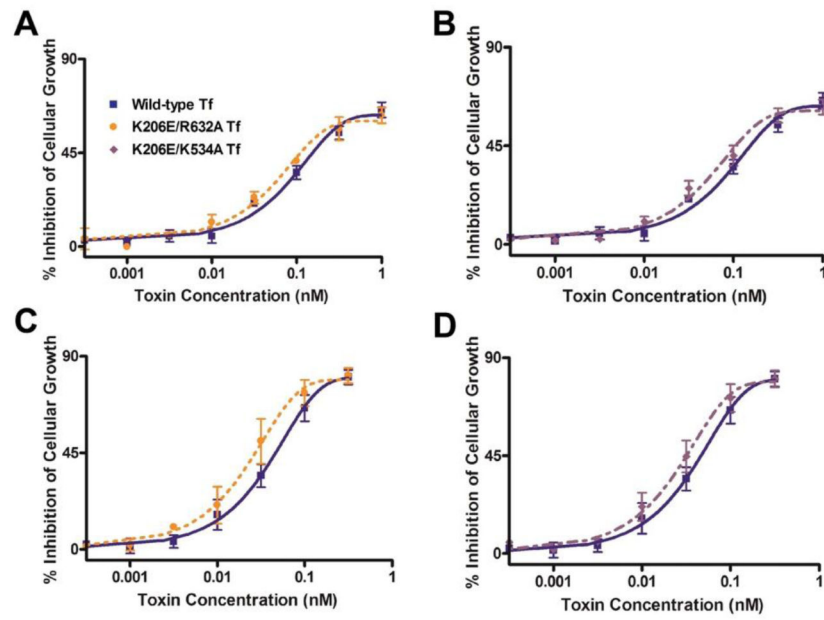


**Figure 6.** *In vitro* cytotoxicity comparisons for CRM107 conjugates for non-neoplastic cells. Points, mean from an average of three experiments; bars, standard deviation. Wild-type Tf versus K206E/R632A Tf and K206E/R534A Tf in (A, B) HUVECs and (C, D) NHAs.

**Table 1**

List of parameters in the DT/DTR intracellular trafficking model.

Rate Constant	Definition	Value	Ref.
$k_{DT}$	Association rate constant of DT for DTR	$1.90 \times 10^7 \text{ M}^{-1} \text{ min}^{-1}$	Est.
$k_{DT,r}$	Dissociation rate constant of DT for DTR	$1.90 \times 10^{-2} \text{ min}^{-1}$	Est.
$k_{int,DT}$	Internalization rate constant	$2.8 \times 10^{-2} \text{ min}^{-1}$	Est.
$k_{trans}$	Endosomal translocation rate constant	$1.5 \times 10^{-1} \text{ min}^{-1}$	Est.
$k_{lys}$	Endosome to lysosome rate constant	$1.8 \times 10^{-1} \text{ min}^{-1}$	Est.
$k_{deg}$	Degradation rate constant	$4.0 \times 10^{-2} \text{ min}^{-1}$	Est.
$f_{DT}$	Fraction of internalized DT sorted for translocation	$3.33 \times 10^{-1}$	(Dorland et al., 1979)
$n_{cell}$	Cell number	$4.75 \times 10^5 \text{ cells}$	(Papini et al., 1993)
$V_{bulk}$	Bulk media volume	$5 \times 10^{-4} \text{ L}$	(Papini et al., 1993)
$N_A$	Avogadro's number	$6.02 \times 10^{23} \text{ mol}^{-1}$	N/A

**Table 2**

List of parameters in the Tf-DT conjugate intracellular trafficking model.

Rate Constant	Definition	Value	Ref.
$k_{FeTf}$	Association rate constant of FeTfDT for TfR	$(9.6 \pm 0.2) \times 10^7 \text{ M}^{-1} \text{ min}^{-1}$	(Lebron et al., 1998)
$k_{FeTf,r}$	Dissociation rate constant of FeTfDT for TfR	$(7.8 \pm 1.2) \times 10^{-2} \text{ min}^{-1}$	(Lebron et al., 1998)
$k_{Tf}$	Association rate constant of TfDT for TfR	$0 \text{ M}^{-1} \text{ min}^{-1}$	(Lebron et al., 1998)
$k_{Tf,r}$	Dissociation rate constant of TfDT for TfR	$2.6 \text{ min}^{-1}$	(Ciechanover et al., 1983)
$k_{DT}$	Association rate constant of (Fe)TfDT for DTR	$1.90 \times 10^7 \text{ M}^{-1} \text{ min}^{-1} \text{ }^a$ $2.375 \times 10^3 \text{ M}^{-1} \text{ min}^{-1} \text{ }^b$	Est.
$k_{DT,r}$	Dissociation rate constant of (Fe)TfDT for DTR	$1.90 \times 10^{-2} \text{ min}^{-1}$	Est.
$k_{endo}$	Endosomal association rate constant of (Fe)TfDT for TfR	$(4.4 \pm 0.4) \times 10^7 \text{ M}^{-1} \text{ min}^{-1}$	(Lebron et al., 1998)
$k_{endo,r}$	Endosomal dissociation rate constant of (Fe)TfDT for TfR	$(5.6 \pm 1.2) \times 10^{-2} \text{ min}^{-1}$	(Lebron et al., 1998)
$k_{int,Tf}$	TfR-mediated internalization rate constant	$2.0 \times 10^{-1} \text{ min}^{-1}$	(Ciechanover et al., 1983)
$k_{int,DT}$	DTR-mediated internalization rate constant	$2.8 \times 10^{-2} \text{ min}^{-1}$	(Dorland et al., 1979)
$k_{Fe,rel}$	Endosomal Tf iron release rate constant	$1.0 \times 10^2 \text{ min}^{-1} \text{ }^c$ $1.0 \times 10^{-3} \text{ min}^{-1} \text{ }^d$	Est.
$k_{trans}$	Vesicle to cytosol translocation rate constant	$1.5 \times 10^{-1} \text{ min}^{-1}$	Est.
$k_{sv}$	TfR-mediated degradation rate constant	$1.2 \times 10^{-1} \text{ min}^{-1}$	(French and Lauffenburger, 1997)
$k_{st}$	TfR-mediated tubule to recycling rate constant	$5.3 \times 10^{-1} \text{ min}^{-1}$	(French and Lauffenburger, 1997)
$k_{deg,Tf}$	TfR-mediated degradation rate constant	$6.0 \times 10^{-2} \text{ min}^{-1}$	(French and Lauffenburger, 1997)
$k_{rec}$	TfR-mediated recycling rate constant	$1.5 \times 10^{-1} \text{ min}^{-1}$	(French and Lauffenburger, 1997)
$\kappa$	Vesicle/tubule partition coefficient	0.44	Est.
$\eta$	Tubule to vesicle volume ratio	0.43	(French and Lauffenburger, 1997)
$\gamma$	TfR-mediated vesicle to tubule rate constant	$1.0 \text{ min}^{-1}$	(French and Lauffenburger, 1997)
$k_{lys}$	DTR-mediated vesicle to lysosome transfer rate constant	$1.8 \times 10^{-1} \text{ min}^{-1}$	Est.
$k_{deg,DT}$	DTR-mediated degradation rate constant	$4.0 \times 10^{-2} \text{ min}^{-1}$	Est.
$f_{DT}$	Endosome to cytosol translocation fraction	0.33	(Dorland et al, 1979)
$n_{cell}$	Cell number	$4 \times 10^5$ cells	N/A
$V_{bulk}$	Bulk media volume	$1 \times 10^{-3} \text{ L}$	N/A
$V_{endo}$	Endosomal volume	$1.0 \times 10^{-14} \text{ L}$	(French and Lauffenburger, 1997)
$N_A$	Avogadro's number	$6.02 \times 10^{23} \text{ mol}^{-1}$	N/A

<sup>a</sup>Wild-type DT<sup>b</sup>CRM107<sup>c</sup>Wild-type Tf<sup>d</sup>Mutant Tf

**Table 3**  
**Simulation IC<sub>50</sub> values of DT conjugates versus CRM107 conjugates**

Mutant Tf conjugates exhibit improved efficacy compared to their wild-type Tf counterparts. Changing the toxin moiety to CRM107 results in an improved fold difference between the mutant Tf and the wild-type Tf conjugates.

Conjugate	IC <sub>50</sub> (pM)	IC <sub>50</sub> decrease associated with mutant Tf
<b>DT conjugates</b>		
Wild-type Tf-DT	13.4	
Mutant Tf-DT	8.66	1.5-fold
<b>CRM107 conjugates</b>		
Wild-type Tf-CRM107	36.8	
Mutant Tf-CRM107	8.20	4.5-fold

Author Manuscript

Author Manuscript

Author Manuscript

Author Manuscript

**Table 4**  
**IC<sub>50</sub> values of various Tf-CRM107 conjugates in cancerous cell lines**

The IC<sub>50</sub> values of Tf-CRM107 conjugates are listed for U87, U251, and HeLa cells. SD, standard deviation. Mutant Tf-CRM107 conjugates exhibit improved efficacy compared to wild-type Tf-CRM107 conjugates.

Cell Line	IC <sub>50</sub> ± SD (pM)	Average IC <sub>50</sub> decrease associated with mutant Tf
<b>U87</b>		
Wild-type Tf-CRM107	32.1 ± 3.2	
K206E/R632A Tf-CRM107	7.10 ± 0.87	~4.6 fold
K206E/K534A Tf-CRM107	6.80 ± 0.52	
<b>U251</b>		
Wild-type Tf-CRM107	35.3 ± 3.7	
K206E/R632A Tf-CRM107	10.9 ± 1.8	~3.2 fold
K206E/K534A Tf-CRM107	11.3 ± 1.2	
<b>HeLa</b>		
Wild-type Tf-CRM107	30.3 ± 3.0	
K206E/R632A Tf-CRM107	9.4 ± 1.0	~3.0 fold
K206E/K534A Tf-CRM107	10.2 ± 1.4	

**Table 5**  
**Simulation IC<sub>50</sub> values of mutant Tf-CRM107 conjugates in neoplastic versus non-neoplastic cells**

Results demonstrate that a decreased number of TfR results in an increased IC<sub>50</sub> value and reduced cytotoxicity.

TfR Number	IC <sub>50</sub> (pM)
<b>Neoplastic cells</b>	
$5.4 \times 10^5$	8.20
<b>Non-neoplastic cells</b>	
$5.4 \times 10^4$	11.5
$2.97 \times 10^4$	16.4
$5.4 \times 10^3$	81.0
$2.97 \times 10^3$	144.4

**Table 6**  
***In vitro* IC<sub>50</sub> values of Tf-CRM107 conjugates with non-neoplastic cells**

The IC<sub>50</sub> values for mutant CRM107 against non-neoplastic cells are much higher than against neoplastic cell lines, suggesting a good therapeutic index.

Cell Line	IC <sub>50</sub> ± SD (pM)
<b>HUVEC</b>	
Wild-type Tf-CRM107	195 ± 30
K206E/R632A Tf-CRM107	147 ± 36
K206E/K534A Tf-CRM107	136 ± 24
<b>NHA</b>	
Wild-type Tf-CRM107	55.0 ± 9.3
K206E/R632A Tf-CRM107	32.4 ± 7.4
K206E/K534A Tf-CRM107	38.0 ± 6.8

Author Manuscript

Author Manuscript

Author Manuscript

Author Manuscript